Design of a truth sensor for the GMT laser tomography adaptive optics system

Marcos A. van Dam,[a] Rodolphe Conan,[b] Antonin H. Bouchez,[c] and Brady Espeland[b]

[a]Flat Wavefronts, P.O. Box 1060, Christchurch 8140, New Zealand;
[b]Research School of Astronomy & Astrophysics, Australian National University, Cotter Rd., Weston, ACT 2611, Australia;
[c]Giant Magellan Telescope Observatory Corporation, P.O. Box 90933, Pasadena, CA 91109, USA

ABSTRACT

The GMT laser tomography adaptive optics (LTAO) system design has a truth sensor guiding on a natural guide star. The truth sensor is used to measure telescope segment piston errors and measure slowly varying non-common path aberrations. The challenge lies in measuring segment piston using faint natural guide stars and the wavefront delivered by the LTAO system. This requires a sensor that can make a direct phase measurement. It is demonstrated that an infrared, AO-corrected, unmodulated pyramid or roof wavefront sensor can make the required measurements at 10 Hz for stars brighter than magnitude 17 at H- or K-band.

Keywords: Adaptive optics, Giant Magellan Telescope, simulations, wavefront sensing, pyramid wavefront sensor, segment piston

1. INTRODUCTION

Adaptive optics (AO) has found widespread use in astronomical settings to compensate for atmospheric turbulence and telescope aberrations. Almost all of the current generation of 8-10 m telescopes are equipped with AO. Studies are under way to design the AO systems for the next generation of telescopes: the Thirty Meter Telescope (TMT), the European Extremely Large Telescope (E-ELT) and the Giant Magellan Telescope (GMT).

The Giant Magellan Telescope[1] will have three AO modes at first light:[2] a ground layer adaptive optics (GLAO) system[3] to improve the seeing over a large field and over the whole sky, a laser tomography adaptive optics (LTAO) system[4] for diffraction-limited performance over almost the whole sky, and a natural guide star adaptive optics (NGS AO) system[5] for excellent correction around bright stars. In every mode, the correction is applied with an adaptive secondary mirror (ASM).

A particular feature of the GMT design is that it has seven segments with large gaps between them, as shown in Figure 1. The ASM is also segmented, with the same geometry as the primary mirror.

The pupil segmentation leads to two sources of segment piston error: the telescope component, caused by incorrect positioning of either the primary or secondary mirror segments, and the atmospheric component, which is the difference in segment piston between the reconstructed wavefront and the true wavefront.[6] Wavefront sensors based on geometric optics, such as the laser guide star (LGS) Shack-Hartmann wavefront sensors, are unable to measure any piston error between the segments and employ a reconstructor to produce the smoothest possible wavefront that is consistent with the wavefront sensor measurements. Since the true wavefront is not, in general, as smooth as the reconstructed wavefront, there is an error in estimating the piston terms even if there is no noise in the measurements. In this paper, we limit our discussion to measuring segment piston for the LTAO system of the GMT. For a discussion on how the pyramid wavefront sensor in the NGS AO system measures segment piston, the reader is referred to Esposito *et al.*[5] Changes in segment piston have only a small impact on GLAO and seeing-limited observations, and no segment piston sensor is planned.

The LTAO system uses six laser guide stars (LGSs) in a regular hexagon to probe the 3D structure of the atmosphere.[4] The LGSs are launched from three different locations on the side of the telescope. A natural guide

Further author information: send correspondence to Marcos van Dam, marcos@flatwavefronts.com

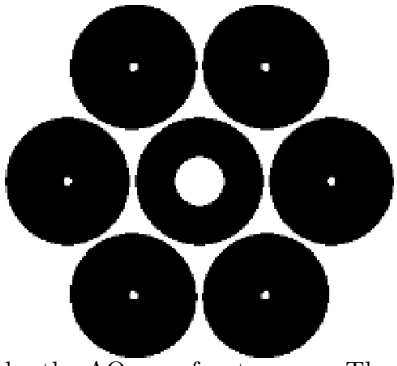

Figure 1: Effective GMT pupil as seen by the AO wavefront sensor. The tilt of the off-axis segments leads to an elliptical pupil image for these segments and to a widening of the gap between the segments.

star is also needed in order to make tip-tilt measurements at 500-1000 Hz and detect changes in focus due to altitude fluctuations in the sodium layer at about 10 Hz. The current design calls for an off-axis infrared tip-tilt star behind a deformable mirror (DM) that corrects for anisoplanatism.

Existing LGS AO systems with side-launched LGSs use a truth sensor to measure aberrations due to the changing structure of the sodium layer.[7] Unfortunately, wavefront sensors looking at LGSs launched from different locations experience different aberrations and consequently the tomographic reconstruction of the LGS aberrations varies with field angle. The resulting aberrations cause not only an error in the on-axis reconstruction, resulting in the wrong shape on the ASM, but also on the off-axis reconstruction, used to drive the DM, and the truth sensor is unable to distinguish between the two. Therefore, the LTAO wavefront sensor is designed to adequately sample even the most elongated spots in order to minimize the LGS aberrations.[4]

This paper deals with the design of a truth sensor for the LTAO system. In addition to segment piston, the truth sensor is required to measure any slowly-varying aberrations due to non-common path errors which change with changing sodium altitude and pupil angle. If the truth sensor is able to run at 10 Hz, it can also be used as the focus sensor.

The remainder of the paper is organized as follows. There is a discussion of the segment piston requirements in Sect. 2. Sect. 3 studies of the ability of different sensors to measure segment piston. Monte-Carlo simulations are presented in Sect. 4, followed by a conclusion in Sect. 5.

2. SEGMENT PISTON ERROR SENSING REQUIREMENTS

In this section, we describe the two sources of segment piston error: the telescope and the atmosphere.

2.1 Telescope segment piston

An important problem in the design of the GMT is how to keep the telescope phased. A complex phasing system has been designed and is explained in detail elsewhere.[8–10] To summarize, it consists of the following:

- A phasing camera using bright off-axis guide stars with a large capture range
- Fine edge sensors for the primary mirror using a distance measuring interferometer
- Coarse edge sensors for the primary mirror using an absolute image encoder
- Edge sensors for the secondary mirror using a pair of differential capacitive plates

The main limitation of the design is the timescale over which the primary mirror fine edge sensor mounting locations drift, due to thermal effects, with respect to the optical surface. If just one segment experiences an 0.1° C change in front-to-back gradient, the displacement of the bosses with respect to the optical surfaces will

be interpreted as a change in relative piston of 45 nm. Analysis shows that the fine edge sensors should generally remain sufficiently stable for about five minutes. The truth sensor needs to have a closed-loop bandwidth no longer than this timescale, corresponding to an update rate of 30 s or less. The solution to this problem is to use AO-corrected infrared light to measure segment piston.

2.2 Atmospheric segment piston

The atmospheric turbulence profile used in this paper is the median profile from Goodwin's thesis,[11] and reproduced in Table 1. The value of r_0 at 500 nm is 0.151 m.

Altitude (m)	25	275	425	1250	4000	8000	13000
Cn2 ($\times 10^{-13}$m$^{1/3}$)	0.4393	0.3054	0.2328	1.2228	0.7947	0.2381	0.2627
Wind speed (ms^{-1})	5.65	5.80	5.89	6.64	13.29	34.83	29.42
Wind direction (°)	0.8	8.3	12.5	32.5	72.1	93.2	100.1

Table 1: Median seeing for Las Campanas Observatory reported by Goodwin.[11]

The atmospheric segment piston error changes quickly and must be measured and corrected at a bandwidth greater than 250 Hz, as shown in Table 2.

Frame rate (Hz)	1000	250	100	40	0
RMS wavefront error (nm)	10	39	113	137	144

Table 2: Atmospheric segment piston error as a function of frame rate for the case of median seeing.

Table 3 demonstrates that a star near the optical axis must be used. Since it is only possible to measure segment piston using a bright, on-axis guide star, the atmospheric component of the segment piston error can only be measured and corrected in NGS AO mode.

Off-axis distance (arcsec)	0	10	20	30	No sensor
RMS wavefront error (nm)	0	58	113	165	144

Table 3: Atmospheric segment piston error as a function of off-axis distance for the case of median seeing.

Note that for an LTAO system, the magnitude of the atmospheric segment piston error is reduced relative to its value for an NGS system (shown in Tables 2 and 3) because only the low altitude layers contribute to this error; the overlap of the metapupils at high altitude turbulent layers means that there is no "gap" in the wavefront estimates.

3. PHASE SENSORS

A truth sensor that can measure phase directly (rather than just the phase slope or curvature) is needed to measure the segment piston. The ESO Active Phasing Experiment made a comparison of a number of candidates in the context of the European ELT.[12] It appears from their results that the pyramid sensor makes the most sensitive measurement of segment piston. The problem for the GMT is more difficult, because the segment gaps are orders of magnitude larger. To make matters worse, any tip-tilt in the primary mirror, conjugate to the ground, that is corrected by tilting the corresponding ASM segment, conjugate to 200 m, leads to an off-axis piston error, so we need a star as close to on-axis as possible. A number of options have been considered. Interferometric methods, such as the Zernike phase sensor (Fig. 2),[13] have a limited dynamic range and were found to require a flatter wavefront than is produced by the LTAO system. Simulations using phase diversity showed that focal plane methods require stars much brighter than we have at our disposal. Here, we present two wavefront sensors that were found to be suitable: the pyramid sensor and the closely related roof sensor.

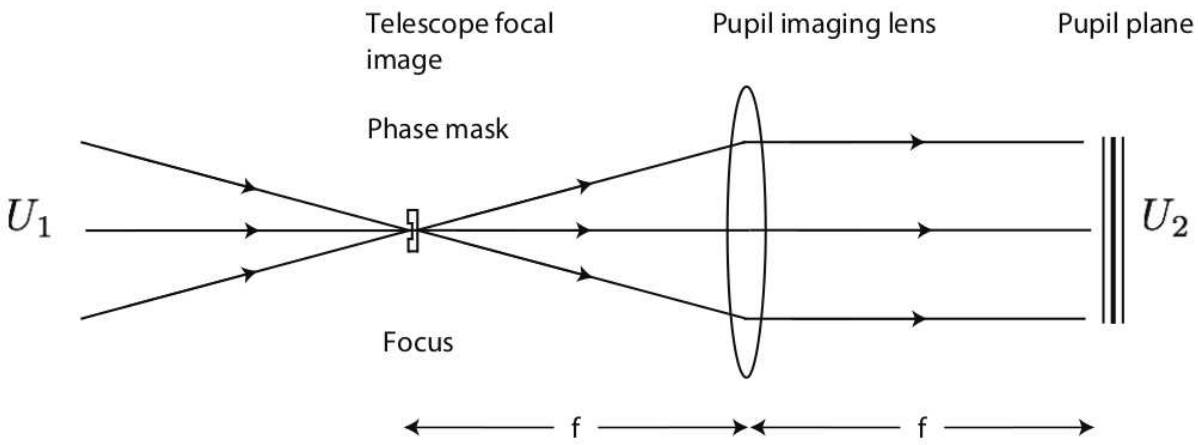

Figure 2: A schematic of the Zernike phase sensor.[12] A phase mask with a $\lambda/4$ retardation outside the center is placed at the focal plane. In the pyramid wavefront sensor, the phase mask is replaced by a four-sided pyramid. In the roof sensor, the phase mask is replaced by two orthogonal two-sided prisms.

3.1 Phase measurements with the pyramid sensor

The pyramid wavefront sensor was first proposed by Ragazzoni as an alternative to the Shack-Hartmann wavefront sensor.[14] It consists of a four-sided pyramid at the focal plane and a zoom lens to reimage four pupils onto a detector. The sensitivity of the pyramid can be traded off against dynamic range by modulating the pyramid (steering the pyramid or the image around the focal plane).

The pyramid sensor was subsequently found to have other desirable properties, such as excellent noise propagation,[15,16] and the ability to change the spatial sampling on the fly. More importantly for our purposes, it was shown to act as a phase sensor as well as a phase slope sensor under certain circumstances.[17,18] The response of the pyramid sensor to a poked GMT segment is shown in Fig 3. In the literature, there are two ways to

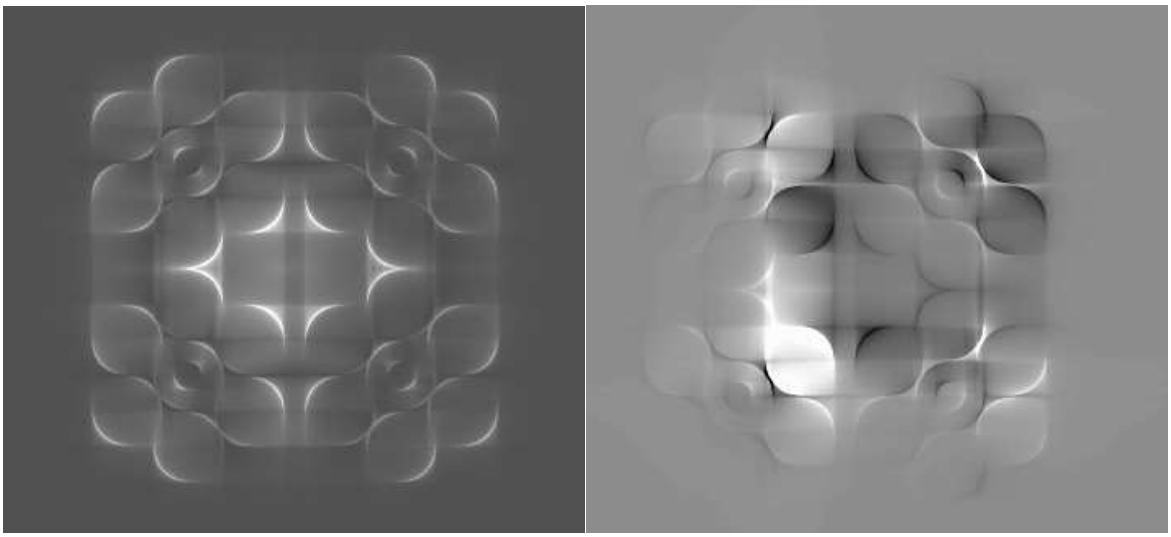

(a) (b)

Figure 3: Reponse of the pyramid sensor to a 0.2 radian poke of the top right hand segment: (a) the intensity of the four subimages and (b) the difference in intensity between the images with and without a poked segment.

process the intensity of the four subimages. The first is to treat the four subimages like the four pixels of a Shack-Hartmann wavefront sensor:[14,19]

$$s_x(x,y) = \frac{I_1(x,y) + I_2(x,y) - I_3(x,y) - I_4(x,y)}{I_1(x,y) + I_2(x,y) + I_3(x,y) + I_4(x,y)} \tag{1}$$

and

$$s_y(x,y) = \frac{I_1(x,y) - I_2(x,y) + I_3(x,y) - I_4(x,y)}{I_1(x,y) + I_2(x,y) + I_3(x,y) + I_4(x,y)}, \tag{2}$$

where $s_x(x,y)$ and $s_y(x,y)$ are the x and y-centroids at location (x,y) and $I_j(x,y)$ corresponds to location (x,y) of the j^{th} subimage.

An alternative way to process the images is to replace the denominator with an average subaperture intensity (where the average is both spatial and temporal) as the denominator.[16] Both formulations have been experimented with, and it is not yet clear which formulation is better for segment piston sensing. In this report, we use Eqs. (1) and (2).

Most existing pyramid sensors use modulation and it is interesting to see what the effect of modulation on the signal produced by poking a segment is (Fig. 4). When there is no modulation, the signal can be detected

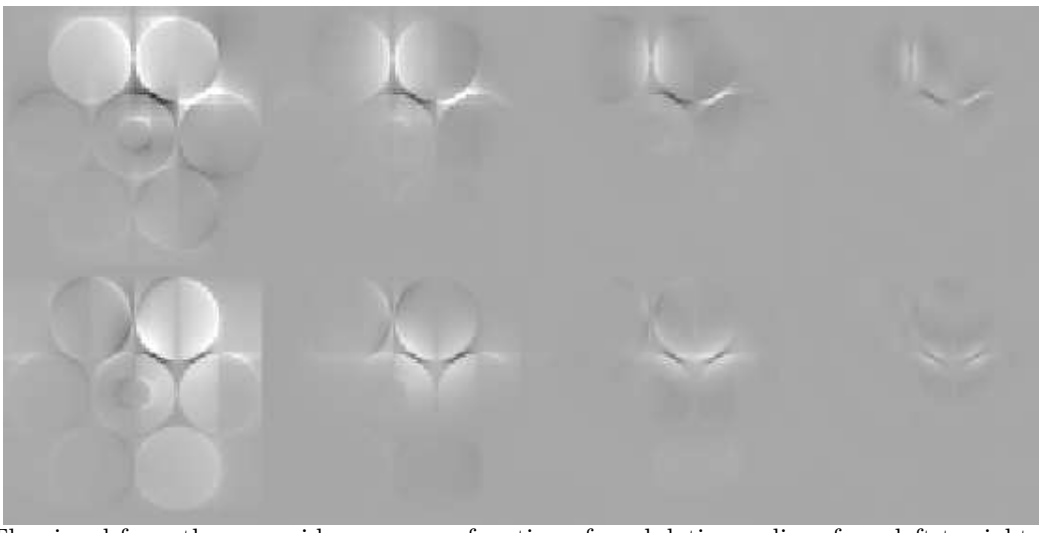

Figure 4: The signal from the pyramid sensor as a function of modulation radius: from left to right, 0, 1, 2 and 4 λ/D. The top signal represents s_x and the bottom signal s_y. The top right hand segment is poked by $\lambda/10$ relative to the other segments.

over a large fraction of the pupil. This permits the use of a few large pixels and a relatively low number of photons are needed to detect the piston. As the modulation amplitude increases, the strength of the signal produced by a segment piston error decreases and becomes more localized in and near the gap between the segments. If modulation is required, we would be forced to use a detector with a larger number of pixels and a longer integration time. Modulation of the pyramid is typically needed for two reasons: (i) the wavefront sensor saturates because the wavefront aberration exceeds the dynamic range of the sensor and (ii) because the edges of the pyramid cannot be fabricated to be sufficiently sharp. Fortunately, by sensing an AO-corrected wavefront at infrared wavelengths, we can avoid problems with saturation. The difficulty in fabricating a pyramid with sharp edges can be mitigated by replacing the four faces of a pyramid by a sensor that has two sets of two faces: the roof sensor.

3.2 Phase measurements with the roof sensor

The roof sensor replaces the pyramid of the pyramid sensor by two sets of prisms which are rotated at 90° relative to each other. The light is split into two beams of equal intensity, with half the light focused on the edge of

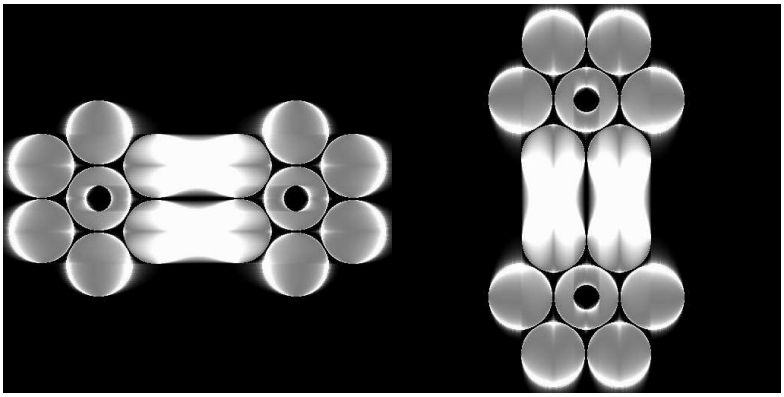

(a) (b)

Figure 5: Images produced by a roof sensor: (a) the x-channel and (b) the y-channel.

each prism. The pupils are reimaged, as shown in Fig. 5. The signal processing is similar to the pyramid sensor, except that the two channels are analyzed separately:

$$s_x(x,y) = \frac{I_1(x,y) - I_2(x,y)}{I_1(x,y) + I_2(x,y)} \tag{3}$$

and

$$s_y(x,y) = \frac{I_3(x,y) - I_4(x,y)}{I_3(x,y) + I_4(x,y)}. \tag{4}$$

For the roof sensor, using mean subaperture values for the denominator did not produce good results.

The roof sensor was tested on the bench by Riccardi *et al.* while they were waiting for the pyramid to be fabricated.[20] Subsequent theoretical studies have shown that a roof sensor is more sensitive than a pyramid.[21,22]

Here, we analyze its applicability to sensing segment piston. The signals produced when one segment is poked, displayed in Fig 6, demonstrate that the roof sensor produces very clean signals when a phase discontinuity is present and, at least in theory, appears to be the ideal sensor to be used as the truth sensor.

4. MONTE-CARLO SIMULATIONS

4.1 Simulation description

Simulations were run in YAO to verify the performance of the truth sensor under realistic simulation conditions. YAO is an end-to-end Monte-Carlo simulation tool written in Yorick with a large and flexible feature set.[23] A description of how to model the GMT LTAO system was presented elsewhere.[6] Three thousand iterations of the LGS WFS loop of the LTAO system were run, representing six seconds of simulation time. The residual wavefront from the LTAO system is used as the input to the truth sensor. The other input is a fictitious segment piston error, as shown in 7. The RMS telescope segment piston is 250 nm of wavefront, with a maximum of 400 nm and an average of 0 nm. The maximum difference between two segments of 600 nm. The pyramid sensor is modeled as follows. First, a Fourier transform is taken of the complex amplitude at the pupil plane, to obtain the complex amplitude at the focal plane. A pyramidal phase retardation is added at the focal plane to model the pyramid. To model modulation, this phase is displaced by a number of discrete points in a circle around the focal plane. Finally, the inverse Fourier transform is taken to obtain four subimages. The roof sensor is modeled in the same way, except that the beam is first split into two channels and two prisms take the place of the pyramid. A much faster, but less accurate, way to model the pyramid is to divide the light at the focal plane into four quadrants and take the inverse Fourier transform of each one separately. This removes any interaction between the four subpupils and is effectively modeling a pyramid with a very steep vertex.

Two sampling modes were used: a 10x10 and 35x35 sampling across the pupil. In both cases, the output of the truth sensor was used to estimate the segment piston error as well as the first 45 Zernike modes. It is essential

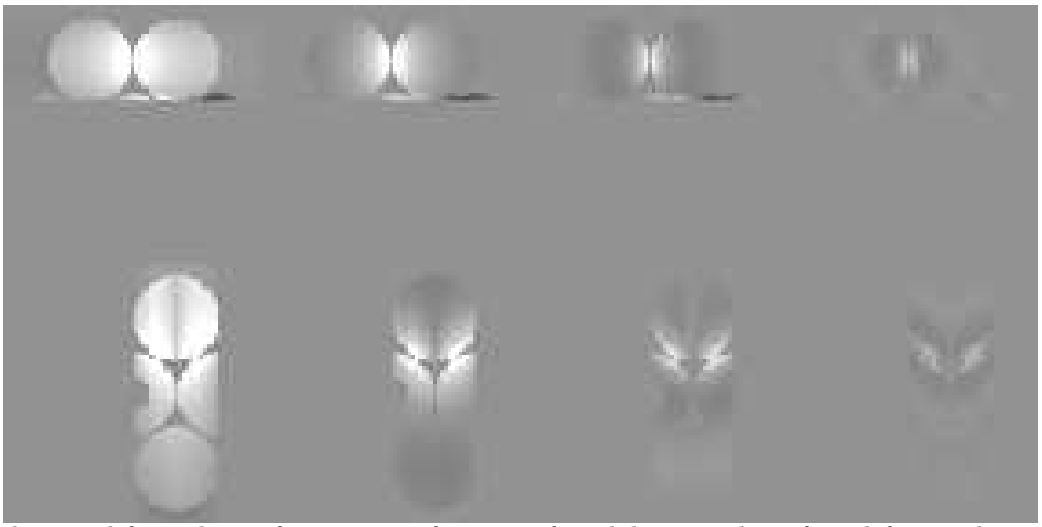

Figure 6: The signal from the roof sensor as a function of modulation radius: from left to right, 0, 1, 2 and 4 λ/D. The top signal represents s_x and the bottom signal s_y. The top right hand segment is poked by $\lambda/10$ relative to the other segments.

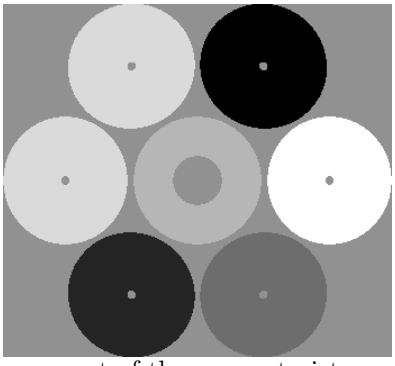

Figure 7: The telescope component of the segment piston assumed in the simulations.

to also fit and correct low-order modes because otherwise they can alias onto segment piston. For example, a focus error can be partially corrected by moving the central segment relative to the outer segments. The frame rate of the truth sensor was set to 10 Hz. This is fast enough to keep up with changes in the sodium altitude if the truth sensor also acts as a focus sensor.

The use of the truth sensor as a segment piston sensor was evaluated by comparing its performance to that of an ideal segment piston sensor, which simply averages the phase over each segment.

The atmospheric conditions, unless specifically mentioned, were assumed to be the median profile presented in Table 1.

4.2 Bright, on-axis guide stars

Initially, the best case scenario was simulated. This comprises of a bright, on-axis tip-tilt star at zenith, which was also used to measure segment piston. In this case, the LGS and tip-tilt WFSs were assumed to be noiseless for speed of simulaton. The on-axis Strehl ratio delivered by the LTAO system, without any telescope segment piston, is 0.707 at K-band and 0.554 H-band. If segment piston is present and uncorrected, these values drop to 0.428 and 0.248 respectively. For this case, it was found that all configurations were able to measure segment piston without any need for modulation, as shown in Table 4. An interesting point to note is that using a truth

Segment piston sensor	Ideal	Pyramid		Roof	
Sampling		10×10	35×35	10×10	35×35
K-band	0.724	0.723	0.728	0.723	0.719
H-band	0.721	0.710	0.717	0.707	0.699

Table 4: K-band Strehl ratio delivered by on-axis truth sensor for a number of different noiseless truth sensors in median seeing (r_0=0.151 m).

sensor actually increases the Strehl ratio compared to the case with no segment piston. This is due to the fact that wavefront modes invisible to the LTAO are sensed by the truth sensor.

The obvious question is what happens when the seeing degrades, or the correction degrades for other reasons. As a first experiment, the residual wavefront was doubled, which corresponds to an r_0 of 0.100 m at 500 nm. The K- and H-band Strehl ratios delivered by the LTAO system are now 0.273 and 0.116 without any telescope segment piston and 0.181 and 0.063 with telescope segment piston. The results are tabulated in Table 5. There is

Segment piston sensor	Ideal	Pyramid		Roof	
Sampling		10×10	35×35	10×10	35×35
K-band	0.295	0.267	0.289	0.282	0.273
H-band	0.296	0.132	0.258	0.235	0.234

Table 5: K-band Strehl ratio delivered by on-axis truth sensor for a number of different noiseless truth sensors in twice the median seeing (r_0=0.100 m).

a large drop in performance for the 10x10 pyramid sensor at H-band, and this is caused by interference between the pupils. Using a steeper pyramid, which leads to a larger separation of the reimaged pupils on the detector, results in improved performance when the residual turbulence is high.

4.3 Faint, on-axis guide stars

Since the tip-tilt sensor and the truth sensor look at the same star, there is anisokinetism (tip-tilt anisoplanatism) to contend with. Nevertheless, the star will move around due to measurement noise and bandwidth error on the tip-tilt measurement. The simulations were run with the median seeing residuals along with a tip-tilt error of 10 mas RMS along each axis, representing the worst case scenario. It can be seen from Table 6 that the tip-tilt error does not appear to affect the ability to measure segment piston.

Segment piston sensor	Ideal	Pyramid		Roof	
Sampling		10×10	35×35	10×10	35×35
K-band	0.279	0.249	0.274	0.273	0.274
H-band	0.280	0.150	0.263	0.262	0.263

Table 6: K-band Strehl ratio delivered by on-axis truth sensor for a number of different noiseless truth sensors in median seeing (r_0=0.151 m). The tip-tilt error is random and has a value of 10 mas RMS along each axis.

4.4 Limiting magnitude

In order to meet the sky coverage requirements, the truth sensor must be able to operate with faint guide stars. Ideally, we would like the truth sensor to operate at 10 Hz in order to make focus measurements fast enough to track changes in the sodium layer altitude. Simulations were run to assess the performance as a function of guide star magnitude. The photometric and noise parameters used in the simulations are tabulated in Table 7. A square field stop was used with length $10\lambda/D$. The simulation results as a function of guide star magnitude are displayed in Fig. 8. Phillion and Baker found that the noise on the roof sensor is a factor of $\sqrt{2}$ times better than for the case of the pyramid sensor,[21] and this was borne out by the simulations here. There is also a slight

Parameter	H-band	K-band
Wavelength (μm)	1.654	2.179
Photometric zero point	1.1×10^{12}	0.70×10^{12}
Sky and telescope background (mag/arcsec^2).	13.7	13.4
Quantum efficiency	0.4	0.4
Dark current	0	0
Read-out noise (e-)	4	4

Table 7: Parameters used in the simulations that affect the measurement noise.

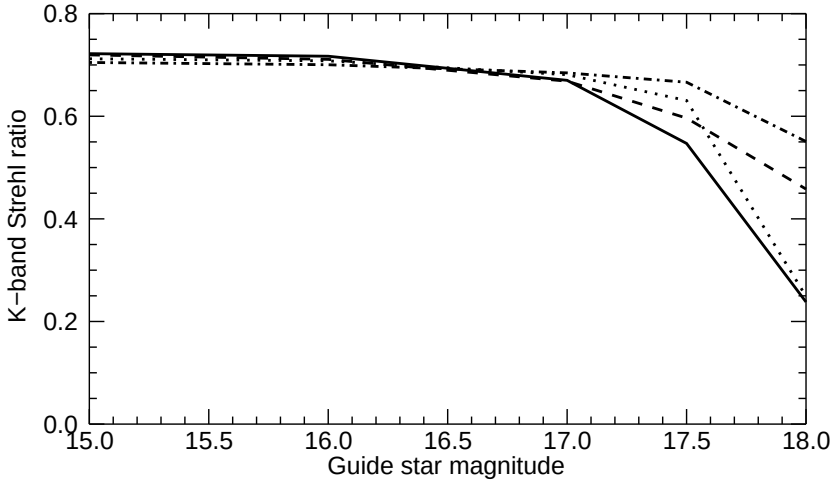

Figure 8: K-band Strehl ratio as a function of guide star magnitude for the K-band pyramid (solid) and roof (dash-dot) sensor, H-band pyramid (dot) and roof (dash) sensors in median seeing (r_0=0.151 m)

advantage to selecting the H-band over the K-band. It can be seen that the pyramid sensor can be used for 17^{th}-magnitude stars at 10 Hz; fainter stars could be accommodated by reducing the loop gain and/or the frame rate.

5. CONCLUSION AND DISCUSSION

In this article, we investigate possibility of using an infrared pyramid or roof wavefront sensor as the truth and segment piston sensor for the LTAO system of the GMT. Both wavefront sensors can measure segment piston under ideal, diffraction-limited conditions, but the signal for the roof sensor is much cleaner. In both cases, modulation of the spot around the focal plane has the effect of reducing the sensitivity to segment piston and localizing the signal to the region around the segment gap.

In the case where the tip-tilt star is on-axis and median seeing conditions are present, the segment piston is easily measured and corrected using H- or K-band light. When the turbulence is doubled, the performance of the segment piston sensor is compromized, particularly at the shorter wavelength. The reason for this is that the segment piston measurement is affected by the turbulence residuals. Future work will consider how to make the segment piston measurement at low to modest Strehl ratios. In the work presented, the interaction matrices between the segment piston and the wavefront sensor were calibrated under diffraction-limited conditions, which clearly do not apply in the low Strehl ratio regime. A non-linear reconstruction of the pyramid sensing signal could overcome this problem. Under these conditions, the performance was found to improve by spacing out the reimaged pupils in order to reduce the level of cross-talk betweem them.

The truth and segment piston sensor can operate with faint guide stars. The tip-tilt residuals produced by guiding on a faint tip-tilt star were shown not to inhibit the performance of the sensors. While the roof sensor is

less sensitive to noise than the pyramid, both sensors have very good sensitivity and can operate at 10 Hz using stars as faint as 17^{th}-magnitude, allowing us to use the truth sensor as a focus sensor as well.

ACKNOWLEDGMENTS

This work has been supported by the GMTO Corporation, a non-profit organization operated on behalf of an international consortium of universities and institutions: Astronomy Australia Ltd, the Australian National University, the Carnegie Institution for Science, Harvard University, the Korea Astronomy and Space Science Institute, the Smithsonian Institution, The University of Texas at Austin, Texas A&M University, University of Arizona and University of Chicago. This material is based in part upon work supported by AURA through the National Science Foundation under Scientific Program Order No. 10 as issued for support of the Giant Segmented Mirror Telescope for the United States Astronomical Community, in accordance with Proposal No. AST-0443999 submitted by AURA.

REFERENCES

[1] M. Johns *et al*, "Giant Magellan Telescope: overview," Proc. SPIE **8444-52** (2012).

[2] A. H. Bouchez *et al*, "The Giant Magellan Telescope adaptive optics program", SPIE **8447-54** (2012).

[3] P. M. Hinz *et al*, "Design and Predicted Performance of the GMT Ground-Layer Adaptive Optics System, Proc. SPIE **8447-137** (2012).

[4] R. Conan *et al*, "The Giant Magellan Telescope laser tomography adaptive optics system," Proc. SPIE **8447-135** (2012).

[5] S. Esposito *et al*, "Wavefront sensor design for the GMT natural guide star AO system," Proc. SPIE **8447-57** (2012).

[6] M. A. van Dam *et al*, "Modeling the adaptive optics systems on the Giant Magellan Telescope," Proc. SPIE **7736-42** (2010).

[7] R. M. Clare, M. A. van Dam and A. H. Bouchez, "Modeling low order aberrations in laser guide star adaptive optics systems," Opt. Express **15**, 4711-4725 (2007).

[8] "Phasing System Conceptual Design Report," GMT Technical Report GMT-AO-DOC-00266, Rev 0.2 (2012).

[9] A. H. Bouchez *et al*, "The Giant Magellan Telescope phasing system," Proc. SPIE **8447-138** (2012).

[10] D. S. Acton *et al*, "Phasing metrology system for the GMT," Proc. SPIE **8444-75** (2012).

[11] M. S. Goodwin, "Turbulence profiling at Siding Spring and Las Campanas Observatories," Ph.D. Thesis, Australian National University (2009).

[12] I. Surdej, "Co-phasing segmented mirrors: theory, laboratory experiments and measurements on sky," PhD thesis, Ludwig-Maximilians-Universitat Munchen (2011).

[13] E. E. Bloemhof and J. K. Wallace, "Simple broadband implementation of a phase contrast wavefront sensor for adaptive optics," Optics Express **12**, 6240-6245 (2004).

[14] R. Ragazzoni, "Pupil plane wavefront sensing with an oscillating prism," J. Mod. Opt. **43**, 289293 (1996).

[15] O. Guyon, "Limits of adaptive optics for high-contrast imaging," ApJ **629** 592 (2005).

[16] S. Esposito and A. Riccardi, "Pyramid Wavefront Sensor behavior in partial correction Adaptive Optic Systems," Astron. Astrophysics **369** L9 (2001).

[17] C. Verinaud, "On the nature of the measurements provided by a pyramid wave-front sensor," Optics Communications **233**, 27-38 (2004).

[18] L. Johnson *et al*, "Pyramid wavefront sensing: theory and component technology development at LAO," Proc. SPIE **6272**, 62724R (2006).

[19] D. Peter *et al*, "PYRAMIR: Exploring the On-Sky Performance of the Worlds First Near-Infrared Pyramid," PASP **122** 63-70 (2010).

[20] A. Riccardi *et al*, " Laboratory characterization of a "Foucault-like" wavefront sensor for Adaptive Optics," Proc. SPIE **3353**, 941-951 (1998).

[21] D. Phillion and K. Baker, "Two-sided pyramid wavefront sensor in the direct phase mode" Proc. SPIE **6272** (2006).

[22] J. Wang *et al*, "Comparison between non-modulation four-sided and two-sided pyramid wavefront sensor," Optics Express **18**, 27534-27549 (2010).

[23] https://github.com/frigaut/yao.